Check for updates

View Article Online
View Journal

Journal of
Materials Chemistry C

Accepted Manuscript

This article can be cited before page numbers have been issued, to do this please use: Y. Wu, Q. Zhang, J. Li, X. Tian, D. Li, X. Lu, B. Xu, Y. Wu and K. Guo, *J. Mater. Chem. C*, 2019, DOI: 10.1039/C8TC06109B.

Volume 4 | Number 1 | 7 January 2016 | Pages 1–224

Journal of Materials Chemistry C
Materials for optical, magnetic and electronic devices
www.rsc.org/MaterialsC

ISSN 2050-7526

ROYAL SOCIETY OF CHEMISTRY

PAPER
Nguyễn T. K. Thanh, Xiaodi Su et al
Fine-tuning of gold nanorod dimensions and plasmonic properties using the Hofmeister effects

175 YEARS

This is an Accepted Manuscript, which has been through the Royal Society of Chemistry peer review process and has been accepted for publication.

Accepted Manuscripts are published online shortly after acceptance, before technical editing, formatting and proof reading. Using this free service, authors can make their results available to the community, in citable form, before we publish the edited article. We will replace this Accepted Manuscript with the edited and formatted Advance Article as soon as it is available.

You can find more information about Accepted Manuscripts in the author guidelines.

Please note that technical editing may introduce minor changes to the text and/or graphics, which may alter content. The journal's standard Terms & Conditions and the ethical guidelines, outlined in our author and reviewer resource centre, still apply. In no event shall the Royal Society of Chemistry be held responsible for any errors or omissions in this Accepted Manuscript or any consequences arising from the use of any information it contains.

ROYAL SOCIETY OF CHEMISTRY

rsc.li/materials-c

View Article Online
DOI: 10.1039/C8TC06109B

Journal Name

ARTICLE

Regulation of dithiafulvene-based molecular shape and their aggregations on TiO_2 for high efficiency dye-sensitized solar cells

Received 00th January 20xx,
Accepted 00th January 20xx

DOI: 10.1039/x0xx00000x

www.rsc.org/

Yuezhen Wu,[a] Quande Zhang,[b] Jie Li,[a] Xia Tian,[a] Da Li,[a] Xiaoqing Lu,[b] Bingshe Xu,[a] Yucheng Wu,[a] Kunpeng Guo*[a]

A well-matched relationship between the molecular shape and the aggregations of donor-π-acceptor (D-π-A) organic dyes is of great significance for understanding the principle of maximizing the performance of dye-sensitized solar cells (DSCs). To this end, two dithiafulvene-based organic sensitizers with different molecular shapes were synthesized, and the influence of their aggregations formed on TiO_2 on the diversity performance of DSCs were investigated. It was found that V-shaped **DTF-C5** with a larger flare angle of 150.6° between the donor and acceptor unit in molecular sturcture tend to form compact aggregates on the surface of TiO_2 without the loss of adsorbed dyes, thus giving a higher short-circuit density (J_{sc}) of 14.92 mA cm^{-2} and a power conversion efficiency (PCE) of 7.39%, which were 1.48-fold and 1.53-fold higher than those of the DSC with CDCA co-adsorbent, respectively. On the other hand, **DTF-C6** possessing a typical V-shaped conformation with a flare angle of 120.6° needed to co-adsorb with CDCA to fill up the vacant sites between the dye aggregates on the TiO_2 surface, aiming to reduce the current loss and suppress the electron recombination. Compared to the DSC with pristine **DTF-C6** aggregation, that based on the co-adsorbed system dramatically uplifted the PCE from 5.50% to 9.04%, owing to the improved J_{sc} and open-circuit voltage. This work presents a perspective of rational regulation on molecular shapes and dye aggregations of organic dyes for highly efficient DSCs.

Introduction

Converting solar energy into electricity through photovoltaic (PV) technologies has attracted huge attention to tackle the issues of environmental pollution and the shortage of fossil fuels supply.[1-3] Among the emerging PV technologies, dye-sensitized solar cells (DSCs) show fascinating prospects due to their advanced features, such as handy device fabrication, environmental friendliness, low production cost and fascinating performance under indoor conditions with low-intensity light.[4-7] To improve the performance of DSCs, enormous efforts in sensitizing dyes innovation and devices engineering have been made by the worldwide researches.[8-12] Recently, donor-π-acceptor (D-π-A)-type organic dyes have exhibited merits to promote the performance of DSCs, including flexibility in molecular designing, high molar extinction coefficient and favourable charge injection from dyes to photonanode.[13-16] For example, employing *N*-annulated perylene as donative building blocks for DSCs, a power conversion efficiency (PCE) over 12% was realized in Wang's group.[17] Through collaborative sensitization by a carbazole and a triphenylamine based D-π-A dyes, a recorded PCE of 14.3% was realized in Yano and Hanaya's group.[18] In addition to the mostly used arylamine derivatives sensitizing dyes, our group also found dithiafulvene based D-π-A dyes could be effective sensitizers for high-performance DSCs, owing to their excellent electron-donative characteristic and more concise synthesis.[19-23]

To date, studies have found there are two primary means for realizing high PCE in DSCs, one is enhancing the short-circuit density (J_{sc}) and the other is improving the open-circuit voltage (V_{oc}).[24-29] In principle, the J_{sc} can be enhanced by broaden the absorption spectra of dyes via strengthening the intramolecular charge transfer (ICT) effect with suitable molecular engineering.[30-33] Thereby, various enlarged conjugation of D-π-A organic dyes with different shapes have been studied. However, larger conjugated frameworks are susceptible to dye-aggregation after absorbing on the surface of TiO_2, and may lead to vacant sites between the dye aggregates. In this case, V_{oc} would be decreased due to the adverse electron recombination, and even current loss was found due to the limited charge transfer and injection.[34-38] To tackle this issue, researchers resorted to introduce coadsorbents, *e.g.*, chenodeoxycholic acid (CDCA),[39-41] onto the vacant sites of TiO_2 surface, or design organic dyes with large steric hindrance (*e.g.* star-shaped dyes).[42-45] However, some organic dyes with reduced steric hindrance, which are more prone to form aggregates, were also

---

[a] *Ministry of Education Key Laboratory of Interface Science and Engineering in Advanced Materials, Research Center of Advanced Materials Science and Technology, Taiyuan University of Technology, Taiyuan 030024, China. *E-mail: guokunpeng@tyut.edu.cn*
[b] *School of Materials Science and Engineering, China University of Petroleum, Qingdao, Shandong 266580, China*
Electronic Supplementary Information (ESI) available: ^{1}H NMR. See DOI: 10.1039/x0xx00000x

Published on 15 January 2019. Downloaded on 1/22/2019 4:29:40 AM.

Journal of Materials Chemistry C Accepted Manuscript

Please do not adjust margins

View Article Online
DOI: 10.1039/C8TC06109B

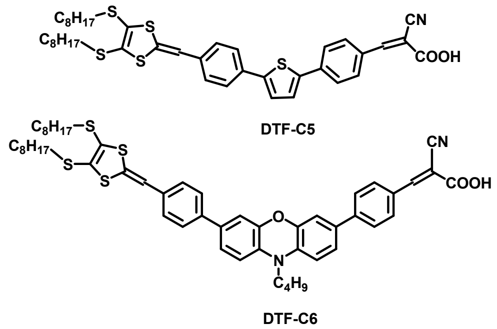

Fig. 1 Chemical structures of dyes **DTF-C5** and **DTF-C6**.

reported yielding high efficiencies in DSCs without using coadsorbents.[46,47] These results indicate molecular shapes and aggregations of organic dyes exert great influence on DSCs' performance. However, systematic studies on the relationship between molecular conformations and dye aggregations in one dye system to maximize the performance of DSCs remain relatively rare.

In this research, two D-π-A dithiafulvene-based organic sensitizers with the same electron donor and acceptor units but differing in the flare angles induced by the π-bridges were designed and synthesized (Fig. 1), respectively. **DTF-C5** with phenyl-thiophene-phenyl π-bridge and **DTF-C6** with phenyl-phenoxazine-phenyl π-bridge showed similar absorption spectra in solution, which were beneficial to evaluate the effect of molecular shapes and dye aggregations on the DSCs' performance. The influence of their CDCA- co-adsorption-dependent aggregations on TiO_2 surface on the performance of DSCs was investigated. The DSC fabricated with pristine **DTF-C5** displayed a far higher PCE of 7.39% than that with CDCA co-adsorbent due to the compact arrangement of the sensitizers. Interestingly, for the typical V-shaped molecule with a reduced flare angle, **DTF-C6** based DSCs achieved a dramatically increased PCE of 9.04% with the co-adsorption of CDCA to cover the vacant sites between the dye aggregates on the TiO_2 surface.

Experimental section

Materials and reagents

All solvents and reagents, unless otherwise stated, were of purist quality and used as received. Phenoxazine, 1-bromobutane, 4-formylphenylboronic acid, tetrakis (triphenylphosphine) palladium (0) ($Pd(PPh_3)_4$), *N*-bromosuccinimide, 2,5-dibromothiophene, and 2-cyanoacetic acid were purchased from Energy Chemical Ltd. FTO conductive glasses (sheet resistance of 15 Ω/sq, Nippon Sheet Glass) were used.

Characterization

NMR spectra (^1H and ^{13}C) measurements were carried out at a Bruker 600 spectrometer in 600 MHz for ^1H NMR and 151 MHz for ^{13}C NMR, respectively, using *d*-chloroform or *d*-DMSO as the solvent. Data was listed in parts per million (ppm) on the delta scale (δ) and coupling constants were reported in Hz. The splitting patterns were designated as follows: s (singlet); d (doublet); t (triplet); q (quartet); m (multiplet) and br (broad). UV-Vis absorption spectra of the dye in solution and loading on TiO_2 films were measured with a HITIACH U-3900 spectrometer at room temperature. Photoluminescent (PL) spectra were recorded in a Horiba Fluoromax 4 spectrometer in diluted THF solution (1×10^{-5} M). Cyclic voltammetry (CV) curve of dye was recorded on a CHI600E Electrochemical Analyzer at a scan rate of 0.1V s^{-1}. The oxidation potential of the sensitizer was measured in DMF with tetra-n-butylammonium hexafluorophosphate ($TBAPF_6$) (0.1 M) as the electrolyte, glassy carbon as the working electrode, Ag/Ag^+ as the reference electrode, and Pt as the counter electrode. The potential of the reference electrode was calibrated with Fc/Fc^+ as an internal reference and converted to normal hydrogen electrode (NHE) by addition of 630 mV.

DSCs fabrication and photovoltaic measurements

The preparation of DSCs photoanode and electrolyte was followed the previous literature.[12] In cell assembly, for the non-coadsorbent devices, **DTF-C5** and **DTF-C6** were loaded onto the TiO_2 (~ 12 μm thick) films by immersion into their tetrahydrofuran (THF) solutions (0.2 mM dye) without the use of CDCA for 24 h at room temperature, respectively. For the coadsorbent based devices, **DTF-C5** and **DTF-C6** were loaded onto the TiO_2 (~ 12 μm thick) film by immersion into their THF solutions (0.5 mM dye) with CDCA (10 mM) for 24 h at room temperature, respectively. Before drying under vacuum, the films were rinsed with acetonitrile to remove the unabsorbed sensitizers multiple times until the solution became clear. Then, the films were assembled into a solar cell together with a Pt–sputtered FTO counter electrode and acetonitrile / valeronitrile (85:15, volume ratio) electrolyte containing 0.6 M 1, 2–dimethyl–3–propylimi dazolium iodide, 0.03 M I_2, 0.1 M guanidinium thiocyanate, and 0.5 M 4–tert-butylpyridine. The active area of the photoanode film for the DSC performance test was typically 0.25 cm^{-2}.

The photocurrent density-voltage (*J-V*) characteristics curves were measured by the Newport PVIV-3A system. The light source (Oriel solar simulator, 450 W Xe lamp, AM 1.5 global filter) was calibrated to 1 sun (100 mW cm^{-2}). Incident Photon to Current Efficiency (IPCE) was measured at varying wavelengths (350-750 nm) with an interval of 5 nm. Nyquist spectroscopy was measured on the electrochemical workstation (Zahner, Zennium) with a frequency response analyzer under an intensity modulated (5-70W m^{-2}) light emitting diode (525 nm) driven by a Zahner (PP211) source supply. The frequency range was set from 100 KHz to 0.1 Hz.

Synthetic procedures

ODT, **C1**, **A** and **B** were obtained as depicted in the previous literature.[19, 48-50]

4,5-bis(octylthio)-1,3-dithiole-2-thione (**ODT**)

1-Bromooctane (6.8 g, 35.0 mmol) and $[Et_4N]_2[Zn(DMIT)_2]$ (5.0 g, 7.0 mmol) were dissolved in CH_3CN (100 mL). Then the reaction mixture was stirred at 80°C for 2 h. After cooling to room temperature, the combined organic extracts were dried over anhydrous $MgSO_4$, filtered, and concentrated under reduced pressure. Compound **ODT** was obtained as yellowish oil by silicon gel column chromatography with petroleum ether as

Published on 15 January 2019. Downloaded on 1/22/2019 4:29:40 AM.

Journal of Materials Chemistry C Accepted Manuscript

This journal is © The Royal Society of Chemistry 20xx

Published on 15 January 2019. Downloaded on 1/22/2019 4:29:40 AM.

Journal of Materials Chemistry C Accepted Manuscript

View Article Online
DOI: 10.1039/C8TC06109B

the eluent (2.7 g, yield 90%). ^{1}H NMR (600 MHz, CDCl$_3$) δ= 2.93–2.81 (m, 3H); 1.66 (dt, J= 15.0, 7.4 Hz, 3H); 1.41 (dt, J= 14.7, 7.3 Hz, 4H); 1.34–1.22 (m, 16H); 0.88 (t, J= 7.0 Hz, 6H).^{13}C-NMR (151 MHz, CDCl$_3$) δ= 213.49; 139.00; 39.67; 35.83; 34.72; 32.64; 32.05; 31.70; 31.47; 31.15; 25.57; 16.98. MALDI-TOF: m/z [M]$^+$ cacld. $C_{19}H_{34}S_5$, 422.7838; found: 422.7836.

4,4'-(10-butyl-10H-phenoxazine-3,7-diyl)dibenzaldehyde (**C2**)

Under a nitrogen atmosphere, 4-formylphenylboronic acid (2.7 g, 22.0 mmol), **B** (4.0 g, 10.0 mmol), Pd(PPh$_3$)$_4$ (0.6 g, 0.5 mmol), K_2CO_3 (6.9 g, 50 mmol) and 1,2-glycol dimethyl ether (DME) (100 mL) were added into a 250 mL three-necked flask. The mixture was stirred at 90°C for 12 h. After cooling to room temperature, the mixture was poured into H_2O, extracted with chloroform and dried over anhydrous MgSO$_4$. After filtration and concentration under reduced pressure, product **C2** was obtained as red solid powder using silica gel column chromatography with petroleum ether:CH$_2$Cl$_2$ (2:1, v:v) as the eluent (2.33 g, 52%). ^{1}H NMR (600 MHz, CDCl$_3$) δ =10.02 (s, 2H); 7.92–7.90 (m, 4H); 7.68–7.66 (m, 4H); 7.14 (dd, *J* = 8.3, 2.2 Hz, 2H); 6.97 (d, *J* = 2.2 Hz, 2H); 6.59 (d, *J* = 8.4 Hz, 2H); 3.58–3.55 (m, 2H); 1.71 (t, *J* = 7.9 Hz, 2H); 1.50 (dt, *J* = 14.8, 7.5 Hz, 2H); 1.05 (t, *J* = 7.4 Hz, 3H). ^{13}C-NMR (151 MHz, CDCl$_3$) δ =194.53; 148.57; 148.04; 137.73; 136.09; 135.26; 133.22; 129.26; 125.62; 116.90; 114.71; 80.14; 79.93; 79.72; 46.81; 30.15; 23.08; 16.79. MALDI-TOF: m/z [M]$^+$ cacld. $C_{30}H_{25}NO_3$, 447.1834; found: 447.1832.

4-(5-(4-((4,5-bis(octylthio)-1,3-dithiol-2-ylidene)methyl)phenyl)thiophen-2-yl)benzaldehyde (**D1**)

Under a nitrogen atmosphere, **ODT** (845.6 mg, 2 mmol) and **C1** (730.0 mg, 2.5 mmol) were dissolved in boiling toluene (20 mL), then P(OEt)$_3$ (5 mL) was added. The resulting mixture was refluxed for 3 h. After cooling and addition of dichloromethane, the mixture was washed with brine and dried over anhydrous MgSO$_4$. Solvents were removed under reduced pressure, and the residue was purified by silica gel column chromatography with petroleum ether: acetic ether (20: 1, v:v) as the eluent to obtain **D1** as yellow solid (373.5 mg, yield 28%). ^{1}H NMR (600 MHz, CDCl$_3$) δ =9.98 (s, 1H); 7.86 (d, *J* = 8.0 Hz, 2H); 7.74 (d, *J* = 7.9 Hz, 2H); 7.60 (d, *J* = 8.1 Hz, 2H); 7.41 (d, *J* = 3.4 Hz, 1H); 7.30 (d, *J* = 2.0 Hz, 1H); 7.22 (d, *J* = 7.8 Hz, 2H); 6.44 (s, 1H); 2.86–2.79 (m, 4H); 1.65 (dq, *J* = 14.7, 7.4 Hz, 4H); 1.46– 1.37 (m, 5H); 1.33–1.25 (m, 17H); 0.88 (q, *J* = 7.1 Hz, 7H). ^{13}C-NMR (151 MHz, CDCl$_3$) δ =194.12; 148.64; 144.38; 142.90; 139.04; 137.98; 136.40; 133.87; 133.36; 130.77; 130.13; 129.05; 128.66; 128.52; 127.78; 127.02; 116.41; 39.06; 34.69; 32.69; 32.02; 31.46; 25.52; 16.94. MALDI-TOF: m/z [M]$^+$ cacld. $C_{37}H_{46}OS_5$, 666.2152; found: 666.2149.

4-(7-(4-((4,5-bis(octylthio)-1,3-dithiol-2-ylidene)methyl)phenyl)-10-butyl-10H-phenoxazin-3-yl)benzaldehyde (**D2**)

Under a nitrogen atmosphere, **ODT** (845.6 mg, 2 mmol) and **C2** (1.1 g, 2.5 mmol) were dissolved in boiling toluene (20 mL), then P(OEt)$_3$ (5 mL) was added. The resulting mixture was refluxed for 3 h. After cooling and addition of dichloromethane, the mixture was washed with brine and dried over anhydrous MgSO$_4$. Solvents were removed under reduced pressure, and the residue was purified by silica gel column chromatography with petroleum ether: acetic ether (20: 1, v:v) as the eluent to obtain **D2** as yellow solid (460.0 mg, yield 28%). ^{1}H NMR (600 MHz, CDCl$_3$) δ = 9.98 (s, 1H); 7.86 (d, *J* = 7.6 Hz, 2H); 7.64 (d, *J* = 7.9 Hz, 2H); 7.49 (d, *J* = 8.4 Hz, 2H); 7.22 (d, *J* = 8.4 Hz, 2H); 7.07 (dd, *J* = 25.1, 9.0 Hz, 2H); 6.91 (d, *J* = 20.1 Hz, 2H); 6.51 (d, *J* = 8.2 Hz, 2H); 6.44 (s, 1H), 3.49 (s, 2H); 2.82 (dd, *J* = 8.2, 6.6 Hz, 4H); 1.64 (d, *J* = 7.1 Hz, 5H); 1.48–1.24 (m, 24H); 1.02 (t, *J* = 7.4 Hz, 3H); 0.87 (q, *J* = 7.1 Hz, 6H). ^{13}C-NMR (151 MHz, CDCl$_3$) δ =194.46; 148.65; 148.10; 147.90; 139.79; 137.90; 137.64; 136.46; 135.08; 134.76; 133.19; 130.58; 130.09; 129.15; 128.89; 127.62; 125.48; 124.70; 116.82; 116.45; 114.67; 114.48; 46.78; 39.04; 34.73; 32.71; 32.07; 31.51; 30.20; 25.56; 23.10; 17.00; 16.82. MALDI-TOF: m/z [M]$^+$ cacld. $C_{49}H_{59}NO_2S_4$, 821.3429; found: 821.3426.

(E)-3-(4-(5-(4-((4,5-bis(octylthio)-1,3-dithiol-2-ylidene)methyl)phenyl)thiophen-2-yl)phenyl)-2-cyanoacrylic acid (**DTF-C5**)

Under a nitrogen atmosphere, **D1** (200.0 mg, 0.3 mmol), cyanoacetic acid (123.2 mg, 1.5 mmol) and piperidine (0.19 mL, 1.9 mmol) were dissolved in CHCl$_3$ (10 mL). The resulting mixture was refluxed for 12 h. After cooling to room temperature, the solvents were removed under reduced pressure, and the residue was purified by silica gel column chromatography with CH$_2$Cl$_2$:CH$_3$OH (10:1, v:v) as the eluent to afford the dye **DTF-C5** as orange yellow solid (132.1 mg, yield 60%). ^{1}H NMR (600 MHz, DMSO) δ =7.89 (s, 1H); 7.87 (d, *J* = 4.5 Hz, 2H); 7.78 (d, *J* = 8.3 Hz, 2H); 7.64 (d, *J* = 8.4 Hz, 2H); 7.61 (d, *J* = 3.8 Hz, 1H); 7.51 (d, *J* = 3.8 Hz, 1H); 7.19 (d, *J* = 8.5 Hz, 2H); 6.66 (s, 1H); 1.93–1.86 (m, 4H); 1.5–1.47 (m, 4H), 1.31–1.28 (m, 4H); 1.15 (d, *J* = 5.9 Hz, 17H); 0.76 (d, *J* = 3.6 Hz, 6H). ^{13}C-NMR (151 MHz, THF) δ= 145.38; 143.11; 141.32; 135.04; 135.02; 132.07; 131.31; 130.25; 129.06; 127.12; 126.32; 125.53; 125.21; 125.02; 124.15; 123.27; 119.02; 113.87; 44.38; 36.73; 32.78; 30.85; 30.58; 30.11; 29.44; 28.25; 23.54; 20.86; 14.45; 14.25. MALDI-TOF: m/z [M]$^+$ cacld. $C_{40}H_{47}NO_2S_5$, 733.2210; found: 733.2208.

(E)-3-(4-(7-(4-((4,5-bis(octylthio)-1,3-dithiol-2-ylidene)methyl)phenyl)-10-butyl-10H-phenoxazin-3-yl)phenyl)-2-cyanoacrylic acid (**DTF-C6**)

Under a nitrogen atmosphere, **D2** (246.0 mg, 0.3 mmol), cyanoacetic acid (123.2 mg, 1.5 mmol) and piperidine (0.19 mL, 1.9 mmol) were dissolved in CHCl$_3$ (10 mL). The resulting mixture was refluxed for 12 h. After cooling to room temperature, the solvents were removed under reduced pressure, and the residue was purified by silica gel column chromatography with CH$_2$Cl$_2$:CH$_3$OH (10:1, v:v) as the eluent to afford the dye **DTF-C6** as red solid (80.0 mg, yield 30 %). ^{1}H NMR (600 MHz, DMSO) δ =7.98 (s, 1H); 7.93 (d, *J* = 7.7 Hz, 2H); 7.75 (d, *J* = 8.2 Hz, 2H); 7.64 (d, *J* = 8.4 Hz, 2H); 7.24 (ddd, *J* = 15.8, 10.3, 5.1 Hz, 4H); 7.05 (dd, *J* = 40.5, 1.8 Hz, 2H); 6.80 (t, *J* = 8.7 Hz, 2H); 6.73 (s, 1H); 3.64 (d, *J* = 6.3 Hz, 2H); 2.89–2.84 (m, 4H); 1.60–1.56 (m, 4H); 1.48–1.21 (m, 24H); 0.97 (t, *J* = 7.3 Hz, 3H); 0.84 (dt, *J* = 12.5, 4.9 Hz, 6H). ^{13}C-NMR (151 MHz, THF) δ =146.07; 143.66; 138.03; 135.91; 134.14; 133.95; 133.00; 132.31; 132.02; 128.78; 128.07; 126.61; 125.73; 123.10; 30.89; 30.72; 30.15; 29.47; 28.26; 23.55; 20.88; 14.46; 14.26. MALDI-TOF: m/z [M]$^+$ cacld. $C_{52}H_{60}N_2O_3S_4$, 888.3487; found: 888.3486.

Published on 15 January 2019. Downloaded on 1/22/2019 4:29:40 AM.

View Article Online
DOI: 10.1039/C8TC06109B

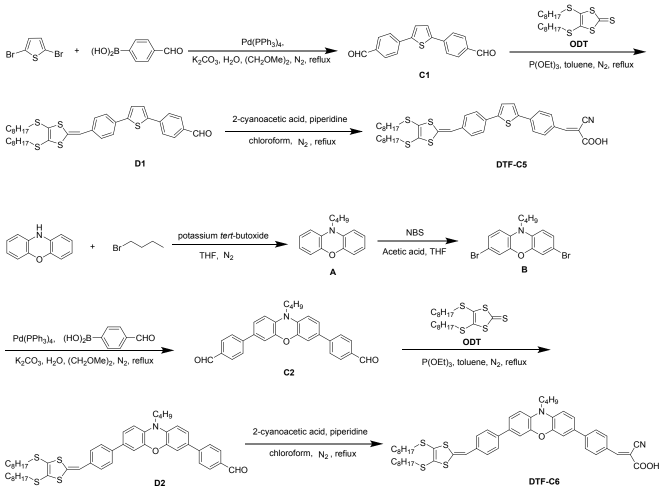

Scheme 1. Synthetic routes to **DTF-C5** and **DTF-C6**.

Results and discussion

Synthesis

The synthesis of **DTF-C5** and **DTF-C6** follow the previously reported stragety.[35] Bromination of compound **A** with NBS produced the brominated phenoxazine derivative **B**. Compound **C2** was obtained by Suzuki reaction of 4-formylphenylboronic acid with **B**. Compounds **C1** and **C2** were then subjected to a phosphite-induced Horner-Wittig condensation with **ODT** to produce the key intermediates **D1** and **D2**. Finally, the π-extend DTF-bearing aldehydes **D1** and **D2** were, respectively, reacted with cyanoacetic acid in the presence of piperidine via the Knoevenagel reaction to give the target sensitizer compounds **DTF-C5** and **DTF-C6**. The chemical structures of **DTF-C5** and **DTF-C6** were fully characterized by ^{1}H NMR, ^{13}C NMR and mass spectrometry. Both **DTF-C5** and **DTF-C6** showed good solubility in common organic solvents such as dichloromethane, tetrahydrofuran (THF) and toluene.

Theoretical calculations

To understand the shapes of the two sensitizers, molecular geometries were first evaluate by density functional theory (DFT) calculations at the B3LYP/6-31G* level using methyl-substituted molecule as the model compound. It was found that **DTF-C5** and **DTF-C6** adopted distinct shapes from each other due to the different π-bridges, as shown in Fig. 2a. Molecule **DTF-C5**, whose π-bridge incorporated two phenyls substitueted at the 2- and 5- positions of the thiophene unit respectively, possessed a larger flare angle of 150.6° between the donor and acceptore units. On the other hand, molecule **DTF-C6**, whose π-bridge incorporated two phenyls substitueted at the 3- and 7- positions of the phenoxazine unit, possessed a typical V-shaped conformation with a smaller flare angle of 120.6°. These results indicate that **DTF-C5** molecules may trend to form more ordered and compact dye aggregates in the solid state compared to **DTF-C6** molecules.

In ordered to understand the photo-induced charge separation of **DTF-C5** and **DTF-C6**, the DFT calculations were performed on electron-density distribution of the HOMOs and LUMOs of the two sensitizers. As shown in Fig. 2b, the HOMO electron density is mainly located at the dithiafulvenyl donor part, while the electron density of LUMO is transferred to the cyanoarylic acid acceptor part. It has demonstrated that the cyanoarylic acid is predominantly adsorbed onto the TiO$_2$ by forming a strong didentate bridging linkage with Brønsted acid sites on the TiO$_2$ surface. Therfore, upon photo-excition, the HOMO-LUMO excitation can efficiently transfer electrons from the donor part to the acceptor part anchored on TiO$_2$, which is desirable for the required charge separation in DSCs.

UV-vis absorption and electrochemical characterization

The UV-Vis absorption spectra of **DTF-C5** and **DTF-C6** in dilute THF solution are shown in Fig. 3a and 3b. The corresponding spectroscopic parameters extracted are summarized in Table 1. The two sensitizers exhibit strong absorption band in the range of 400-450 nm, which can be attributed to the intramolecular charge transfer effect between the donor and acceptor. The absorption maximum (λ_{max}) was observed at 429 nm (molar extinction coefficient ε = 3.90×10^4 M^{-1} cm^{-1}) for **DTF-C5** and 431 nm (ε = 3.10×10^4 M^{-1} cm^{-1}) for **DTF-C6**. The little bathochromic shift of λ_{max} and absorption onset of **DTF-C6** can be attributed to the more electron-rich character of phenoxazinemoiety than that of thiophene.

In comparison with their absorption spectra in THF solution, the profiles of the absorption spectra of TiO$_2$ films (4μm) with these sensitizers loading show dramatically broaden and red-shift absorption, as shown in Fig. 3c. These observations can be related to the formation of aggregates of these sensitizers on the TiO$_2$ surfaces, such as *J*-aggregates. It was also found that the broadened absorption band and the red-shifted absorption onsets by about 100 nm on the thin film should afford increased light harvesting.

The molecular orbital energy levels of **DTF-C5** and **DTF-C6** were derived from CV (Fig. 3d) in combination with the

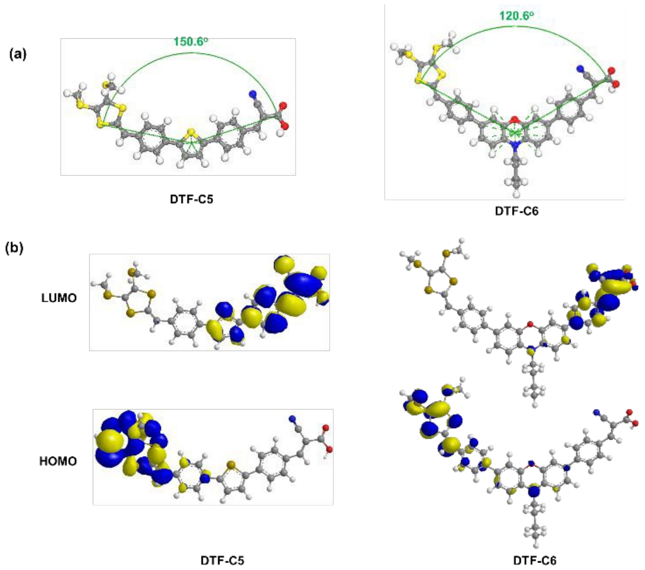

Fig. 2 (a) Optimized molecular geometry of **DTF-C5** and **DTF-C6** based on B3LYP/6-31G* level and (b) Electron-density distributions for the HOMOs and LUMOs of the **DTF-C5** and **DTF-C6**.

Journal of Materials Chemistry C Accepted Manuscript

Please do not adjust margins

View Article Online
DOI: 10.1039/C8TC06109B

Published on 15 January 2019. Downloaded on 1/22/2019 4:29:40 AM.

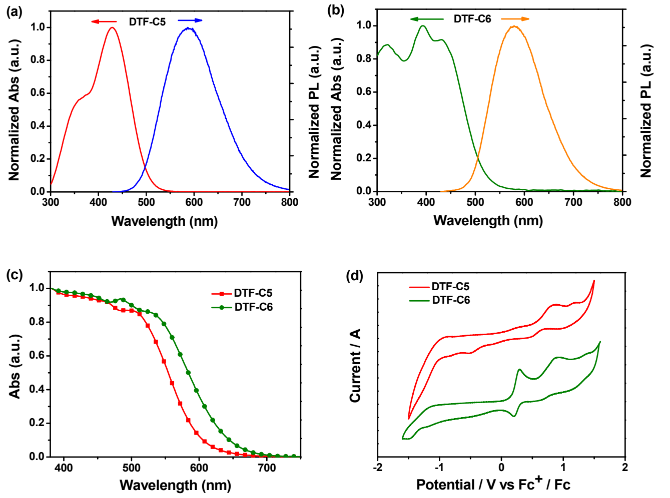

Fig. 3 UV-Vis absorption and PL spectra of (a) **DTF-C5** and (b) **DTF-C6** in dilute THF solution (1×10^{-5} mol L $^{-1}$), (c) normalized UV-vis spectra of **DTF-C5** and **DTF-C6** on TiO_2 films, and (d) Cyclic voltammograms of **DTF-C5** and **DTF-C6** in DMF.

excitation transition energies ($E_{0\text{-}0}$) determined by the intersection of absorption and photoluminescence spectra (Fig. 3a and 3b), and are presented in Table 1. The first oxidation potentials (E_{ox}) of the ground state of **DTF-C5** and **DTF-C6** are corresponding to their highest occupied molecular orbital (HOMO) levels. The E_{ox} of **DTF-C5** and **DTF-C6** was 0.86V and 0.93V, corresponding to HOMO level of -5.26 eV and -5.73 eV, respectively. Obviously, the HOMO levels of the two sensitizers are more positive than the iodide/triiodide couple (0.4 V *vs.* NHE), indicating a thermodynamically downhill regeneration of the photo oxidized sensitizers by accepting electrons from the surrounding I^- ions. The lowest unoccupied orbital (LUMO) energy levels of **DTF-C5** (-1.63 V) and **DTF-C6** (-1.49 V), calculated as E_{ox}-$E_{0\text{-}0}$, are sufficiently negative relative to the conduction-band edge of TiO_2 (-0.5 V *vs.* NHE), ensuring an efficient thermodynamic driving force for the electron injection.

Photovoltaic performance

In order to evaluate the strategy to maximize the performance of DSCs based on organic dyes with different molecular shapes. The devices based the **DTF-C5** and **DTF-C6** absorbedon TiO_2 films with and without CDCA were investigated. The cells were measured under an irradiance of 100 mW cm^{-2}, simulated AM 1.5G sunlight, relevant photovoltaic parameters are collected in Table 2. As shown in Fig. 4a, the champion DSCs based on pristine **DTF-C5** exhibited a J_{sc} and V_{oc} of 14.92 mA cm^{-2} and 759 mV, respectively, combining with a fill factor (*FF*) of 0.65, leading to a high PCE of 7.39%. In contrast, **DTF-C5** co-adsorbed with CDCA (10 mM) based DSCs presented a dramatically decreased PCE of 4.8%, which can be mainly contributed to the decreased J_{sc} and *FF* values (J_{sc}= 10.04 mA/cm^2, and *FF* = 0.61). From Table 2, it could be found that the absorbed amounts of pristine **DTF-C5** in the non-coadsorbent device are higher than those in the CDCA co-adsorbed cells. This result indicates DTF-C5, which adopts a large flare angle and looks like a nearly-linear molecule to some extent, tend to form more ordered and compact aggregates by pristine dye molecules on TiO_2 films. Therefore, comparing to pristine DTF-C5 based DSCs, the DSCs based on DTF-C5 co-adsorbed with CDCA exhibited lower J_{sc} and PCE due to the competive adsorbing of CDCA. However, such results were quite different from the case of DSCs based on **DTF-C6** which possessed a reduced flare angle. As illustrated in Fig. 4b, the DSCs based on pristine **DTF-C6** provide a moderate PCE of 5.5%, with a J_{sc} of 12.44 mA/cm^2, a V_{oc} of 710 mV and a *FF* of 0.62. In comparison with pristine **DTF-C5** based DSCs, such a decreased J_{sc} and V_{oc} of pristine **DTF-C6** based DSCs is counter to their absorption in Fig. 3. However, after co-adsorbing CDCA (10 mM) with **DTF-C6** onto TiO_2 surface, the resulted DSCs dramatically uplift the PCE to 9.04%, accompanied with higher J_{sc} and V_{oc} values (J_{sc}= 15.76 mA/cm^2, and V_{oc} = 790 mV). Considering the absorbed amounts of **DTF-C6** co-adsorbed with CDCA based cells are lower than those in pristine **DTF-C6** based cells (Table 2), it can suggest that the dye-aggregated motifs of pristine **DTF-C5** and **DTF-C6** are different from each other on the TiO_2 surface. There may be more vacant sites on the TiO_2 surface between the **DTF-C6** aggregates. This is because **DTF-C6** adopts a relative smaller flare angle and more twisted molecular strucuture, which supresses compact dye-aggregates forming. To this end, the maximum performance of **DTF-C6** based DSCs can not be presented. Therefore, co-adsorbance with CDCA is necessary for **DTF-C6** to maximize the DSCs' performance as the ingomogeneous distribution of the dye aggregates throughtout the TiO_2 surface would lead to current loss and adverse electron recombination. It was noted that the absorbed amounts of the dye was in the order of pristine dye absorption > with CDCA co-adsorption. However, the J_{sc} values of the DSCs decrease in the order of **DTF-C6** co-adsorbed with CDCA > pristine **DTF-C5** > pristine **DTF-C6** > **DTF-C5** co-adsorbed with CDCA. This result clearly indicates that reasonable regulation of molecular shapes and aggregations on TiO_2 is an important issue to maximum the performance of DSCs.

The incident photon-to-current conversion efficiency (IPCE) spectra shown in Fig. 4 have confirmed the trend of J_{sc} variation.

Table 1 Absorption and electrochemical properties of **DTF-C5** and **DTF-C6**.

Sensitizer	λabs max (nm)	ε (M^{-1} cm^{-1})	E_{ox} (V vs NHE)	$E_{0\text{-}0}$ (ev)	E_{ox}-$E_{0\text{-}0}$ (V vs NHE)	HOMO (ev)	LUMO (ev)
DTF-C5	429	3.90×10^4	0.86	2.49	-1.63	-5.26	-2.77
DTF-C6	431	3.10×10^4	0.93	2.42	-1.49	-5.73	-3.31

Journal of Materials Chemistry C Accepted Manuscript

This journal is © The Royal Society of Chemistry 20xx

View Article Online
DOI: 10.1039/C8TC06109B

Journal Name

ARTICLE

Published on 15 January 2019. Downloaded on 1/22/2019 4:29:40 AM.

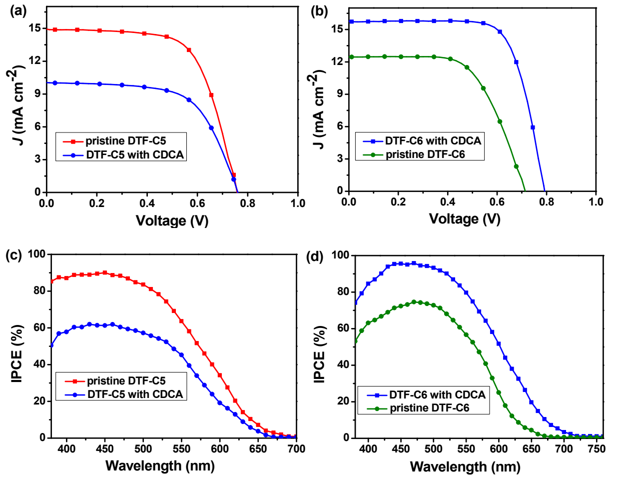

Fig. 4 *J-V* curves of (a) **DTF-C5** and (b) **DTF-C6** based DSCs. Incident photon to current efficiency (IPCE) spectra of (c) **DTF-C5** and (d) **DTF-C6** based DSCs.

Comparing to the DSC based on **DTF-C5** co-adsorbed with CDCA that exhibits a narrow and relatively low IPCE values (slightly higher than 60%), the DSC based on pristine **DTF-C5** exhibits remarkably broadened and increased IPCE (magnitude with values reach 90%) action spectra that covers the visible region. In the case of **DTF-C6**, however, the DSC based on **DTF-C6** co-adsorbed with CDCA gives broader and higher IPCE value (magnitude with values over 95%) than that of pristine **DTF-C6** based DSC. Taken the dye absorbed amounts and molecular shape into together, this difference in IPCE shows that the pristine compact dye aggregates of the **DTF-C5** that with a large flare angle on TiO_2 films lead to enhanced light absorption capabilities and charge carrier injection, thus raising the J_{sc}. On the other hand, the typical V-shaped **DTF-C6** that possesses a reduced flare angle needs the addition of CDCA to fill up the vacant sites between the dye aggregates on the surface of TiO_2, and reduce the current loss.

Electrochemical impedance spectroscopy analysis

To further elucidate the photovoltaic results and display more dynamic information of the interfacial charge transfer process in DSCs sensitized by **DTF-C5** and **DTF-C6** absorbed on TiO_2 films with and without CDCA, electrochemical impedance spectroscopy (EIS) was performed in dark under a forward bias of 0.6 V with a frequency range of 0.1Hz - 100 kHz. Generally, the R_{rec} corresponding to the larger semicircle is related to the charge recombination rate between the TiO_2 film and the electrolyte. In principle, a larger R_{rec} value indicates a slower charge recombination, thus giving a higher V_{oc}. The Nyquist plots for the DSCs based on the sensitizers with or without CDCA co-adsorbent are displayed in Fig. 5. In the case of **DTF-C5**, the R_{rec} values trend in the order of pristine **DTF-C5** > **DTF-C5** co-adsorbed with CDCA, while the trend for **DTF-C6** is turned to**DTF-C6** co-adsorbed with CDCA > **DTF-C6**. These results are in good consistent with the V_{oc} values of the DSCs according to Table 2. Based on these, it can be suggested that compact dye-aggregates of **DTF-C5** form a thick dye layer, thus preventing redox electron acceptors from approaching the TiO_2 efficiently; however, the vacant sites between dye-aggregates of **DTF-C6** need CDCA attendance to eliminate the adverse charge recombination.

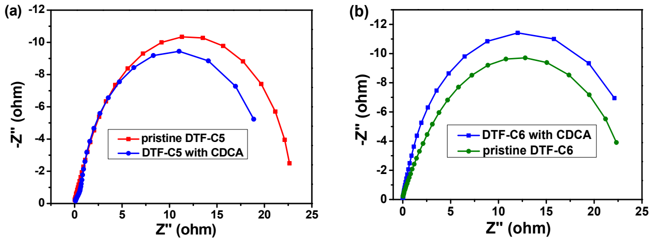

Fig. 5 The Nyquist plots of (a) **DTF-C5** and (b) **DTF-C6** based DSCs.

Conclusion

In summary, two dithiafulvene-based sensitizers **DTF-C5** and **DTF-C6** differing in molecular shapes have been developed to study the relationship between molecular shapes and dye aggregations in one dye system to maximize the performance of DSCs. Our results demonstrate that sensitizer **DTF-C5** with a larger angle between the donor and acceptor units tends to form compact dye-aggregates on the TiO_2 surface without losing the amount of absorbed dyes, passivating the surface to reduce the electron recombination and ensuring optimized *J*sc and V_{oc} values. For typical V-shaped sensitizer **DTF-C6** with a reduced flare angle, it is necessary to introduce CDCA co-adsorbent to fill up the vacant sites between their dye-aggregates to reduce the current loss and electron recombination. As a result, a DSC with a PCE of 7.39% was obtained in the pristine **DTF-C5** based devices. With a little bathochromic absorption, an impressive PCE of 9.04% was realized in **DTF-C6** co-adsorbed with CDCA based DSCs. The primary findings give insights to maximum DSCs performance based on different shape of organic sensitizers.

Journal of Materials Chemistry C Accepted Manuscript

View Article Online
DOI: 10.1039/C8TC06109B

Journal of Materials Chemistry C Accepted Manuscript

Published on 15 January 2019. Downloaded on 1/22/2019 4:29:40 AM.

Table 2 Photovoltaic performance of DSCs based on **DTF-C5** and **DTF-C6**.

Sensitizer	Conc of CDCA	J_{sc} [mA cm^{-2}]	V_{oc} [mV]	*FF*	*η* [%]	Dye absorbed amounts [mol cm^{-2}]
DTF-C5	10mM	10.04±0.15	760±1.4	0.61±0.01	4.80±0.06	(1.95±0.1) ×10^{-7}
DTF-C5	--	14.92±0.21	759±2.2	0.65±0.004	7.39±0.03	(2.68±0.1) ×10^{-7}
DTF-C6	10mM	15.76±0.17	790±1.1	0.72±0.006	9.04±0.04	(2.13±0.1) ×10^{-7}
DTF-C6	--	12.44±0.57	710±0.63	0.62±0.008	5.50±0.02	(2.86±0.1) ×10^{-7}

Conflicts of interest

There are no conflicts to declare.

Acknowledgements

This work was supported by the National Natural Scientific Foundation of China (NO. 21303117, 61605138), the Natural Science Foundation of Shanxi Province (201601D011031, 201601D202030), the Shandong Provincial Natural Science Foundation of China (ZR2017MA024), and the Fundamental Research Funds for the Central Universities (18CX05011A).

References

1 I.-P. Liu, W.-H. Lin, C.-M. Tseng-Shan and Y.-L. Lee, *ACS Appl. Mater. Interfaces*, 2018, **10**, 38900-38905.
2 H. He, C. Zhang, T. Liu, Y. Cao, N. Wang and Z. Guo, *J. Mater. Chem. A*, 2016, **4**, 9362-9369.
3 K. Xie, M. Guo and H. Huang, *J. Mater. Chem. C*, 2015, **3**, 10665-10686.
4 X. Zhang, T. Peng and S. Song, *J. Mater. Chem. A*, 2016, **4**, 2365-2402.
5 M. Pastore, T. Etienne and F. De Angelis, *J. Mater. Chem. C*, 2016, **4**, 4346-4373.
6 X. Zhang, F. Gou, D. Zhao, J. Shi, H. Gao, Z. Zhu and H. Jing, *J. Power Sources*, 2016, **324**, 484-491.
7 M. Pazoki, U. B. Cappel, E. M. J. Johansson, A. Hagfeldt and G. Boschloo, *Energy Environ. Sci.*, 2017, **10**, 672-709.
8 W.-C. Yu, L.-Y. Lin, W.-C. Chang, S.-H. Zhong and C.-C. Su, *J. Power Sources*, 2018, **403**, 157-166.
9 M. Janani, P. Srikrishnarka, S. V. Nair and A. S. Nair, *J. Mater. Chem. A*, 2015, **3**, 17914-17938.
10 P. Chal, A. Shit and A. K. Nandi, *J. Mater. Chem. C*, 2016, **4**, 272-285.
11 K. Li, J. Xu, W. Shi, Y. Wang and T. Peng, *J. Mater. Chem. A*, 2014, **2**, 1886-1896.
12 J. Gao, A. M. El-Zohry, H. Trilaksana, E. Gabrielsson, V. Leandri, H. Ellis, L. D'Amario, M. Safdari, J. M. Gardner, G. Andersson and L. Kloo, *ACS Appl. Mater. Interfaces*, 2018, **10**, 26241-26247.
13 P. Liu, B. Xu, K. M. Karlsson, J. Zhang, N. Vlachopoulos, G. Boschloo, L. Sun and L. Kloo, *J. Mater. Chem. A*, 2015, **3**, 4420-4427.
14 Y. Huang, W.-C. Chen, R. Ghadari, X.-P. Liu, X.-Q. Fang, T. Yu and F.-T. Kong, *J. Power Sources*, 2018, **396**, 559-565.
15 I. Chung, B. Lee, J. He, R. P. H. Chang and M. G. Kanatzidis, *Nature*, 2012, **485**, 486-489.
16 M. J. Ju, I.-Y. Jeon, K. Lim, J. C. Kim, H.-J. Choi, I. T. Choi, Y. K. Eom, Y. J. Kwon, J. Ko, J.-J. Lee, J.-B. Baek and H. K. Kim, *Energy Environ. Sci.*, 2014, **7**, 1044-1052.
17 Z. Yao, M. Zhang, H. Wu, L. Yang, R. Li and P. Wang, *J. Am. Chem. Soc.*, 2015, **137**, 3799-3802.
18 K. Kakiage, Y. Aoyama, T. Yano, K. Oya, J. Fujisawa and M. Hanaya, *Chem. Commun.*, 2015, **51**, 15894-15897.
19 K. Guo, K. Yan, X. Lu, Y. Qiu, Z. Liu, J. Sun, F. Yan, W. Guo and S. Yang, *Org. Lett.*, 2012, **14**, 2214-2217.
20 J. Cheng, Y. Cao, X. Liang, J. Zheng, F. Zhang, S. Wei, X. Lu, K. Guo and S. Yang, *Mater. Chem. Phys.*, 2017, **192**, 349-355.
21 J. Cheng, F. Zhang, K. Li, J. Li, X. Lu, J. Zheng, K. Guo, S. Yang and Q. Dong, *Dyes Pigm.*, 2017, **136**, 97-103.
22 J. Cheng, X. Liang, Y. Cao, K. Guo and W.-Y. Wong, *Tetrahedron*, 2015, **71**, 5634-5639.
23 Y. Cao, J. Cheng, F. Zhang, X. Liang, J. Li, K. Guo and S. Yang, *Sci. China-Mater.*, 2016, **59**, 797-806.
24 C.-C. P. Chiang, C.-Y. Hung, S.-W. Chou, J.-J. Shyue, K.-Y. Cheng, P.-J. Chang, Y.-Y. Yang, C.-Y. Lin, T.-K. Chang, Y. Chi, H.-L. Chou and P.-T. Chou, *Adv. Funct. Mater.*, 2018, **28**, 1703282.
25 L. Favereau, Y. Pellegrin, L. Hirsch, A. Renaud, A. Planchat, E. Blart, G. Louarn, L. Cario, S. Jobic, M. Boujtita and F. Odobel, *Adv. Energy. Mater.*, 2017, **7**, 1601776.
26 Y. P. Fu, H. W. Wu, S. Y. Ye, X. Cai, X. Yu, S. C. Hou, H. Kafafy and D. C. Zou, *Energy Environ. Sci.*, 2013, **6**, 805-812.
27 Y. Yang, H. Zhang, Z.-H. Lin, Y. Liu, J. Chen, Z. Lin, Y. Zhou, C. P. Wong and Z. L. Wang, *Energy Environ. Sci.*, 2013, **6**, 2429-2434.
28 Z. Yao, M. Zhang, H. Wu, L. Yang, R. Li and P. Wang, *J. Am. Chem. Soc.*, 2015, **137**, 3799-3802.
29 D. Moia, T. Leijtens, N. Noel, H. J. Snaith, J. Nelson, P. R. F. Barnes, *Adv. Mater.*, 2015, **27**, 5889-5894.

This journal is © The Royal Society of Chemistry 20xx

View Article Online
DOI: 10.1039/C8TC06109B

Published on 15 January 2019. Downloaded on 1/22/2019 4:29:40 AM.

Journal of Materials Chemistry C Accepted Manuscript

30 J. M. Cole, M. A. Blood-Forsythe, T.-C. Lin, P. Pattison, Y. Gong, Á. Vázquez-Mayagoitia, P. G. Waddell, L. Zhang, N. Koumura and S. Mori, *ACS Appl. Mater. Interfaces*, 2017, **9**, 25952-25961.
31 X. Lu, Y. Shao, S. Wei, Z. Zhao, K. Li, C. Guo, W. Wang and W. Guo, *J. Mater. Chem. C*, 2015, **3**, 10129-10139.
32 J. Cong, X. Yang, L. Kloo and L. Sun, *Energy Environ. Sci.*, 2012, **5**, 9180-9194.
33 G. A. Sewvandi, Z. Tao, T. Kusunose, Y. Tanaka, S. Nakanishi and Q. Feng, *ACS Appl. Mater. Interfaces*, 2014, **6**, 5818-5826.
34 Y. Li, X. Zhang and M. J. Ko, *ACS Sustainable Chem. Eng.*, 2018, **6**, 7193-7198.
35 P. Brogdon, H. Cheema and J. H. Delcamp, *ChemSusChem*, 2017, **10**, 3624-3631.
36 Z. Yang, J. Deng, H. Sun, J. Ren, S. Pan and H. Peng, *Adv. Mater.*, 2014, **26**, 7038-7042.
37 Z. Zhang, X. Chen, P. Chen, G. Guan, L. Qiu, H. Lin, Z. Yang, W. Bai, Y. Luo and H. Peng, *Adv. Mater.*, 2014, **26**, 466-470.
38 T. Chen, L. Qiu, Z. Yang and H. Peng, *Chem. Soc. Rev.*, 2013, **42**, 5031-5041.
39 H. Zhang, Z. Iqbal, Z.-E. Chen and Y. Hong, *Electrochim. Acta*, 2018, **290**, 303-311.
40 W. Ying, F. Guo , J. Li , Q. Zhang, W. Wu, H. Tian, J. Hua, ACS *ACS Appl. Mater. Interfaces,* 2012, **4**, 4215-4224.
41 R. Lin, H. Lin, Y. Yen, C. Chang, H. Chou, P. Chen, C. Hsu, Y. Chen, J. T. Lin, K. Ho, *Energy Environ. Sci.,* 2013, **6**, 2477-2486.
42 A. Michaleviciute, M. Degbia, A. Tomkeviciene, B. Schmaltz, E. Gurskyte, J. V. Grazulevicius, J. Bouclé and F. Tran-Van, *J. Power Sources*, 2014, **253**, 230-238.
43 H. Shahroosvand, P. Abbasi, B. Nemati Bideh, *ChemistrySelect,* 2018, **3**, 6821-6829.
44 M. Urbani, E. M. Barea, R. Trevisan, A. Aljarilla, P. de la Cruz, J. Bisquert, F. Langa, *Tetrahedron Lett.,* 2013, **54**, 431-435.
45 A. Michaleviciute, M. Degbia, A. Tomkeviciene, B. Schmaltz, E. Gurskyte, J. Vidas Grazulevicius, J. Bouclé, F. Tran-Van, *J. Power Sources*, 2014, **253**, 230-238.
46 Y. Ooyama, S. Inoue, T. Nagano, K. Kushimoto, J. Ohshita, I. Imae, K. Komaguchi and Y. Harima, *Angew. Chem. Int. Ed.*, 2011, **50**, 7429-7433.
47 J.-M. Ji, H. Zhou and H. K. Kim, *J. Mater. Chem. A*, 2018, **6**, 14518-14545.
48 W. Lee, J. Choi, J. W. Namgoong, S. H. Kim, K. C. Sun, S. H. Jeong, K. Yoo, M. J. Ko and J. P. Kim, *Dyes Pigm.*, 2014, **104**, 185-193.
49 D. Sipaviciute, D. Tavgeniene, G. Krucaite, D. Volyniuk, J. V. Grazulevicius, B. Yao, Z. Xie, B. Zhang and S. Grigalevicius, *Dyes Pigm.*, 2017, **137**, 208-213.
50 W. Lee, S. B. Yuk, J. Choi, H. J. Kim, H. W. Kim, S. H. Kim, B. Kim, M. J. Ko and J. P. Kim, *Dyes Pigm.*, 2014, **102**, 13-21.

This journal is © The Royal Society of Chemistry 20xx

Please do not adjust margins

View Article Online
DOI: 10.1039/C8TC06109B

Graphical Abstract

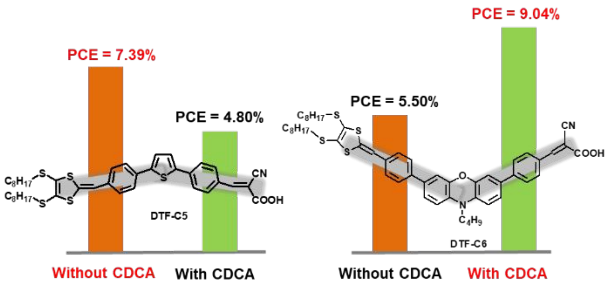

Dithiafulvene-based sensitizers with different flare angles need to coordinate different dye aggregations to maximize the performance of dye-sensitized solar cells.

Published on 15 January 2019. Downloaded on 1/22/2019 4:29:40 AM.

Journal of Materials Chemistry C Accepted Manuscript